



Bistability induced by a spontaneous twisting rate for a two-dimensional intrinsically curved filament

Zicong Zhou *Department of Physics, Tamkang University, New Taipei City, 25137 Taiwan, Republic of China* (Received 30 August 2020; revised 18 November 2020; accepted 6 January 2021; published 19 January 2021)

We find that a moderate intrinsic twisting rate (ITR) can induce a bistable state for a force-free two-dimensional intrinsically curved filament. There are two different configurations of equal energy in a bistable state so that the filament is clearly different from its three-dimensional counterpart. The smaller the ITR or the larger the intrinsic curvature (IC), the clearer the distinction between two isoenergetic configurations and the longer the filament. In bistable states, the relationship between length and ITR is approximately a hyperbola and relationship between IC and critical ITR is approximately linear. Thermal fluctuation can result in a shift between two isoenergetic configurations, but large bending and twisting rigidities can prevent the shift and maintain the filament in one of these two configurations. Moreover, a filament can have a metastable state and at a finite temperature such a filament has the similar property as that of a filament with bistable state.

DOI: [10.1103/PhysRevE.103.012410](https://doi.org/10.1103/PhysRevE.103.012410)

I. INTRODUCTION

Many filamentary materials, such as dsDNA and nanotubes, exhibit finite intrinsic (spontaneous) twisting rate (ITR) [1–34] and/or finite intrinsic curvature (IC) [14–40]. For instance, it is well known that a dsDNA molecule has a large ITR [2,3]. Moreover, special sequence orders favor a finite IC for a short dsDNA chain [16–19]. An example is that tandem sequence repeats of adenine tracts can yield a constant IC in dsDNA [17–19]. It has also been reported that, with a long range correlation in sequence, dsDNA develops a macroscopic (intrinsic) curvature so that the wormlike chain (WLC) model fails to account for its thermal property since the WLC is free of IC and ITR [2,4–6,29]. This should be not a surprise since the long range correlation in sequences tends to make neighbor sequences have similar bending so leads a finite IC. Meanwhile, an intrinsically curved and twisted macroscopic filament is also ubiquitous since a helical spring requires both a finite ITR and a finite IC [24]. These intrinsic parameters are crucial to the structures and functions of filaments [1–24,24–43]. Free of ITR and IC, the natural shape of a filament is a straight line and at a finite temperature (T) the extension of a microscopic filament is a smooth function of stretching force [2,4–6,14]. In contrast, with a finite and constant IC alone the natural shape of a filament is a circle and its extension can subject to a discontinuous transition under a stretching force in both two-dimensional (2D) and three-dimensional (3D) spaces [42,43]. Moreover, it has been reported that an intrinsically curved and twisted filament can form a stable helix and under an applied force the extension of the helix can subject to a discontinuous transition [22–24]. ITR and IC also affect considerably the size or persistence length (l_p) of a microscopic filament [41]. l_p represents an

effective statistical segment length of a coarse-grained model in which one replaces the filament by the trace of a random walk [21]. In other words, l_p is approximately the non-deformable length of a filament, and the mean end-to-end distance and radius of gyration of a long filament are proportional to l_p so that a proper magnitude of l_p is crucial to the function of semiflexible biopolymers [1–14,18–37,39,40].

Moreover, many filaments such as semiflexible biopolymers *in vivo* are in general subjected to various constraints, such as being absorbed on the substrate or moving in a crowd environment. Meanwhile, many devices are in 2D or quasi-2D forms, such as a computer display. A 2D or constrained system often exhibits different property from its 3D counterpart. Therefore, the property of filaments under confinement or in 2D environment has attracted a lot of attentions recently [11,12,44–54].

Theoretical model for a 2D filament usually assumes that the filament is constrained in an ideal 2D plane so that models the filament as a curve of zero cross section and ignores the effect of ITR. However, in practice there is not such an ideal system, and a 2D filament is in fact geometrically constrained or absorbed on a wall or a substrate so that it is uneasy to prohibit the distortion of its cross section. Therefore, ignore ITR completely in 2D case is unreasonable. A finite IC favors a curved shape so tends to reduce the size of either a 2D or 3D filament, but a finite ITR favors a helical shape so tends to enhance the size of a 3D filament [41]. In particular, we should emphasize that in either 3D or ideal 2D case, the natural configuration of a filament, a helix or a circle, is unique so there is not bistable state (BS). Can the cooperation and competition between ITR and IC result in something new and useful in 2D case? In this paper we explore this problem and discover a new bistable mechanism, i.e., a moderate ITR can induce a BS or a bistablelike state (BLS) for a force-free 2D intrinsically curved filament. A BS in this work means that free of external force, i.e., in its natural state, a filament has two distinct stable

*zzhou@mail.tku.edu.tw

configurations of the same energy. Meanwhile, a BLS means that free of external force, besides a ground state configuration (GSC, i.e., the configuration with the lowest energy), the filament has also a metastable configuration with a local minimum energy. Our results reveal that at a finite T , BS and BLS may be indistinguishable so should be equal important.

Bistable materials are ubiquitous and have widely applications such as memory, oscillators, multi vibrators or switches. Moreover, owing to the low energy costing in maintaining colored or colorless state, bistable materials have been regarded as a viable alternative of new display and biomaterial has been considered as a potential material to achieve the goal [55–58]. Therefore, the discovery of a new bistable system and the property of the new system should be very interesting.

The paper is organized as follows. In the next section we set up the model. The Sec. III presents the static equations for GSC and their solutions. The Sec. IV explores the bistable states. The Sec. V studies the effect of a finite T . Finally, the conclusions and discussions conclude the paper in Sec. VI.

II. MODEL

A. Continuous model

In elastic continuous theory, the configuration of a filament can be described by a triad of unit vectors $\{\mathbf{t}_i(s)\}_{i=1,2,3}$ [9,21,23], where $\mathbf{t}_3 = \dot{\mathbf{r}}(s)$ is the unit tangent to the locus of centerline $\mathbf{r}(s)$ of the filament, \mathbf{t}_1 and \mathbf{t}_2 are oriented along the principal axes of the cross section, s is the arclength of the centerline and the symbol “ $\dot{}$ ” represents the derivative with respect to s . The triad obeys the generalized Frenet equations, $\dot{\mathbf{t}}_i = \boldsymbol{\omega} \times \mathbf{t}_i$, where $\boldsymbol{\omega} = \omega_1 \mathbf{t}_1 + \omega_2 \mathbf{t}_2 + \omega_3 \mathbf{t}_3$ is a vector in which ω_1 and ω_2 are components of curvature $c(s)$ or $c^2 = \omega_1^2 + \omega_2^2$, and ω_3 is the twisting rate. Introducing Eulerian angles, we can write [1,7–9,24,59]

$$\mathbf{t}_1 = (\cos \phi \cos \psi - \cos \theta \sin \phi \sin \psi, \sin \phi \cos \psi + \cos \theta \cos \phi \sin \psi, \sin \theta \sin \psi), \quad (1)$$

$$\mathbf{t}_3 = (\sin \phi \sin \theta, -\cos \phi \sin \theta, \cos \theta), \quad (2)$$

$$\omega_1 = \sin \theta \sin \psi \dot{\phi} + \cos \psi \dot{\theta}, \quad (3)$$

$$\omega_2 = \sin \theta \cos \psi \dot{\phi} - \sin \psi \dot{\theta}, \quad (4)$$

$$\omega_3 = \cos \theta \dot{\phi} + \dot{\psi}, \quad (5)$$

and $\mathbf{t}_2 = \mathbf{t}_3 \times \mathbf{t}_1$. The main advantage of using Euler angles is that it is relative easier to find some exact results, as we can see in the next section.

In 2D case, three ω_i s are no longer independent and we can let $\theta = \pi/2$, the angle between \mathbf{t}_3 and x axis is then $\pi/2 - \phi$, so

$$\mathbf{t}_3 = (\sin \phi, -\cos \phi, 0), \quad (6)$$

$$\mathbf{r}(s) = \left(\int_0^L \sin \phi ds, -\int_0^L \cos \phi ds, 0 \right), \quad (7)$$

$$\omega_1 = \sin \psi \dot{\phi}, \quad \omega_2 = \cos \psi \dot{\phi}, \quad \omega_3 = \dot{\psi}. \quad (8)$$

Applying a uniaxial force f (along x axis) at the end of the filament, the energy density owing to the force is $-\mathbf{f} \cdot \mathbf{t}_3 = -f \sin \phi$, so the elastic energy density of an isotropic filament with a finite IC (with components ζ_1 and ζ_2) and ITR (ζ_3) can be written as [9,21,23]

$$\begin{aligned} \mathcal{E} &= \frac{1}{2} \sum_{i=1}^3 b_i (\omega_i - \zeta_i)^2 - f \sin \phi \\ &= \frac{1}{2} [b_1 (\dot{\phi} - c_0 \cos(\psi - \alpha_0))^2 + b_1 c_0^2 \sin^2(\psi - \alpha_0) \\ &\quad + b_3 (\dot{\psi} - \zeta_3)^2 - 2f \sin \phi], \end{aligned} \quad (9)$$

where b_1 is the bending rigidity, b_3 is the twisting rigidity, L is the contour length of the centerline and is a constant so that the filament is inextensible. The magnitude of IC = $c_0 = \sqrt{\zeta_1^2 + \zeta_2^2}$ so we let $\zeta_1 = c_0 \sin \alpha_0$ and $\zeta_2 = c_0 \cos \alpha_0$.

The total energy of the filament is $E = \int_0^L \mathcal{E} ds$. ζ_i can be s dependent but for simplicity we assume that they are s independent, so from Eq. (10) we know that α_0 is irrelevant thus we will ignore it henceforth. b_i and ζ_i represent intrinsic properties of a filament so are independent of T . The end at $s = 0$ of the filament is fixed at $\mathbf{r} = 0$. When $\zeta_1 = \zeta_2 = 0$, it becomes the wormlike rod chain (WLRC) model. Moreover, when $\zeta_1 = \zeta_2 = b_3 = 0$, it is reduced into the WLC model. We should stress that the elastic model can describe both macroscopic and microscopic filaments.

In 3D space and at $f = 0$, the centerline of the GSC given by Eq. (9) is a helix of pitch = $2\pi / (c_0^2 + \zeta_3^2)$ [14,24] so the length of one turn is $L_h = 2\pi / \sqrt{c_0^2 + \zeta_3^2}$.

Due to its slender shape, a semiflexible biopolymer is usually modeled as a filament and elastic models, such as WLC and WLRC models, have been applied to describe successfully the configurations and entropic elasticity of some semiflexible biopolymers [2,4–7,14]. A typical example is dsDNA and for a long dsDNA chain at room temperature $T = T_r = 298$ K, $b_1 = l_p k_B T \approx 50 k_B T_r \cdot \text{nm}$, $b_3 \approx 75 k_B T_r \cdot \text{nm}$ and $\zeta_3 \approx 2\pi / (10.5 * 0.34) \text{nm}^{-1} = 1.76 \text{nm}^{-1}$ [2,3] with k_B the Boltzmann constant and $l_p \approx 50 \text{nm}$ at T_r . However, we should note that these parameters are solution and sample dependent [29,60–62]. For short (<1000 basepairs) dsDNA chain, l_p can be even model dependent and different models can result in very different l_p for a same sample [62].

B. Discrete model

The results from the continuous model indicate that the existence of BS is usually accompanied by a significant change in end-to-end distance. However, the end-to-end distance of a microscopic filament may be sensitive to T since if the energy barrier between two isoenergetic configurations is comparable to $k_B T$, then the filament can shift between isoenergetic configurations frequently. Such a shift may be rather important for the practical applications but it is difficult to estimate the energy barrier in the continuous model. Meanwhile, in general the continuous model represents the limit case of a long filament so that its conclusion may be invalid or demand a correction for a short microscopic filament. But the results obtained from the continuous model reveal that the

BS always occurs at a short filament so that whether the same phenomenon occurs at a microscopic system demands a clarification. Therefore, we discretize the model and perform Monte Carlo simulation with the Metropolis algorithm [63]. In discrete model, a filament consists of N straight and inextensible rods of length d_0 joined end to end. Replacing $\phi(s)$ by ϕ_i , $\psi(s)$ by ψ_i , $\dot{\phi}(s)$ by $(\phi_{i+1} - \phi_i)/d_0$, $\dot{\psi}(s)$ by $(\psi_{i+1} - \psi_i)/d_0$, the reduced energy becomes

$$\begin{aligned} E_T &\equiv E/k_B T \\ &= \frac{1}{2} \sum_{i=1}^{N-1} [k_1(\phi_{i+1} - \phi_i - c_0 \cos \psi_i)^2 + k_1 c_0^2 \sin^2 \psi_i \\ &\quad + k_3(\psi_{i+1} - \psi_i - \zeta_3)^2], \end{aligned} \quad (11)$$

where $k_i \equiv b_i/d_0 k_B T$. We also scale the length by d_0 , i.e., let $d_0 = 1$ so $L = N$ and

$$x_N = x(L) = \sum_{i=1}^N \sin \phi_i, \quad y_N = y(L) = - \sum_{i=1}^N \cos \phi_i. \quad (12)$$

In statistical mechanics, the mean or the thermal average of a physical quantity $B(\phi_i, \psi_i)$ is defined as the average with Boltzmann weights over all possible conformations [63]:

$$\langle B \rangle = \frac{1}{Z} \int d\phi_1 \cdots d\phi_N d\psi_1 \cdots d\psi_N B(\phi_i, \psi_i) e^{-E_T}, \quad (13)$$

$$Z = \int d\phi_1 d\phi_2 \cdots d\phi_N d\psi_1 d\psi_2 \cdots d\psi_N e^{-E_T}. \quad (14)$$

In simulations, we use hinged-hinged boundary conditions (BCs) and equilibrate every sample for 3×10^6 Monte Carlo steps (MCS) before performing average. The hinged-hinged BCs mean that $\phi(0)$, $\phi(L)$, $\psi_0 = \psi(0)$ and $\psi_L = \psi(L)$ are free. The thermal average for a sample are taken from 2×10^7 to 10^8 MCS. Moreover, the initial configuration of every sample is randomly set to avoid bias.

III. STATIC EQUATIONS FOR GSC AND THE GENERAL SOLUTIONS

A. Static equations

In general, the effect of T for a macroscopic filament can be combined into b_i and ζ_i so we can disregard the thermal fluctuation. Moreover, when the thermal fluctuation is negligible, such as at low T or for a short filament with large bending and twisting rigidities, a microscopic filament will stay in its GSC. Therefore, to find GSC is crucial in many cases. Extremizing E , the standard variational method results in the following static equations for the GSC,

$$\frac{\partial \mathcal{E}}{\partial \phi} - \frac{d}{ds} \frac{\partial \mathcal{E}}{\partial \dot{\phi}} = \frac{\partial \mathcal{E}}{\partial \psi} - \frac{d}{ds} \frac{\partial \mathcal{E}}{\partial \dot{\psi}} = 0, \quad (15)$$

and hinged-hinged BCs at $s = 0$ and $s = L$,

$$\partial \mathcal{E} / \partial \dot{\phi} = \partial \mathcal{E} / \partial \dot{\psi} = 0. \quad (16)$$

Explicitly, they are

$$b_1 \ddot{\phi} + b_1 c_0 \sin \psi \dot{\psi} - f \cos \phi = 0, \quad (17)$$

$$b_3 \ddot{\psi} - b_1 c_0 \sin \psi \dot{\phi} = 0, \quad (18)$$

and at both $s = 0$ and $s = L$

$$\dot{\phi} - c_0 \cos \psi = 0, \quad \dot{\psi} - \zeta_3 = 0. \quad (19)$$

When $c_0 = 0$, ψ and ϕ are decoupled and Eqs. (18) and (19) lead to $\psi = \zeta_3 s$ so that ψ makes no contribution to both E and GSC. In this case, the property of the filament has been well studied [48,49]. However, when $\zeta_3 = 0$ it is straightforward to find $\psi = 0$ and the solution of ϕ is the same as that of an ideal 2D filament which has also been well studied [28,29,49,50].

B. The general solutions

Equations (17)–(19) are nonlinear differential equations so that they may have multiple solutions. It is a hard task to solve these equations rigorously when f , c_0 and ζ_3 are all finite. However, we can solve these equation rigorously so to find BS at $f = 0$. In this case, Eqs. (17)–(19) can be integrated once to obtain

$$\dot{\phi} = c_0 \cos \psi, \quad \dot{\psi} = \pm \sqrt{B_1 + B_0 \sin^2 \psi}, \quad (20)$$

where $B_0 = b_1 c_0^2 / b_3$, $B_1 = \zeta_3^2 - B_0 \sin^2 \psi_0$, and $\psi_L = n\pi \pm \psi_0$ with an integer n . Different n therefore offers different branches of solution and clearly a large n allows a large L . But note that no all branches are GSC since some of them may be in local minimum or maximum energy state. Therefore, to find GSC it is also necessary to compare the energies of different branches. In fact, both numerical calculations and computer simulations suggest that there are at most two GSCs.

From Eqs. (10) and (20), we know that ϕ does not contribute explicitly to E in GSC but it determines the shape of GSC. Moreover, Eq. (20) and so ψ depends only on two parameters, B_0 and ζ_3 , so that some properties of GSC are independent of individual b_1 , b_3 and c_0 . In contrast, ϕ and E also dependent on c_0 . Meanwhile, since right sides in Eq. (20) are periodic functions, the negative sign in Eq. (20) and $n < 0$ do not offer any distinct result so we ignore them henceforth.

When $B_1 = 0$, the solution of Eq. (20) is $\sqrt{B_0} s = \log[|\tan(\psi/2)/\tan(\psi_0/2)|]$ and $\sqrt{B_0} L = -2 \log[|\tan(\psi_0/2)|]$. We can expect the similar results when $|B_1/B_0| \ll 1$ and we do not find BS in these cases.

In another limit when $B_0 \ll B_1$, $\sqrt{B_1 + B_0 \sin^2 \psi} \approx \zeta_3$ so from Eq. (20) we obtain $\psi \approx \zeta_3 s + \psi_0$. In this case since in general $\zeta_3 L \neq n\pi$, the BC leads to $\psi_L = \zeta_3 L + \psi_0 = n\pi - \psi_0$ so $\psi_0 = (n\pi - \zeta_3 L)/2$ and $n = \text{Int}(L\zeta_3/\pi)$ with $\text{Int}(v)$ being the integer part of v . Consequently,

$$\phi(s) = \frac{c_0}{\zeta_3} [\sin(\zeta_3 s + \psi_0) - \sin \psi_0] + \pi/2. \quad (21)$$

We also do not find BS in this case.

When $B_1 \neq 0$, Eq. (20) can be integrated into

$$s = \int_{\psi_0}^{\psi} \frac{dv}{\sqrt{B_0 \sin^2 v + B_1}}, \quad (22)$$

$$L = \int_{\psi_0}^{\psi_L} \frac{dv}{\sqrt{B_0 \sin^2 v + B_1}}. \quad (23)$$

If $B_1 < 0$ or ζ_3 is very small, then $\sin^2 \psi_0 \neq -B_1/B_0$, since otherwise $\zeta_3 = 0$. In this case, $n = 0$ or $n > 1$ or $\psi_0 < 0$ or $\psi_L = \pi + \psi_0 \geq \pi$ is prohibited since otherwise

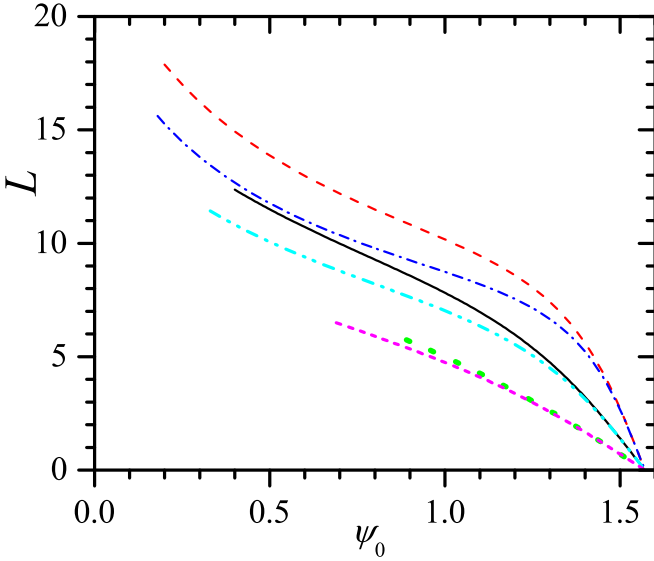


FIG. 1. L vs ψ_0 obtained from Eq. (24) when $B_1 < 0$. $B_0 = 0.067$, $\zeta_3 = 0.05$ (red dashed), 0.1 (solid black) and 0.2 (green dotted); $B_0 = 0.1$, $\zeta_3 = 0.05$ (blue dash-dotted), 0.1 (cyan dash-dot-dotted), and 0.2 (magenta shot-dashed). All ψ_0 s begin from $B_1 \approx 0$. The unit of length is nm so that the units of both c_0 and ζ_3 are nm^{-1} , and the unit of B_0 is nm^{-2} .

$B_0 \sin^2 v + B_1 = B_1 < 0$ at $v = i\pi$ with i being an integer. Therefore, the solution has only one branch with $n = 1$, $\psi_L = \pi - \psi_0$, and

$$L = 2 \int_{\psi_0}^{\pi/2} \frac{dv}{\sqrt{B_0 \sin^2 v + B_1}}. \quad (24)$$

Numerical calculations reveal that L obtained from Eq. (24) is a single-value function of ψ_0 and decreases monotonically with increasing ψ_0 , as shown in Fig. 1 with two different B_0 ($=0.067$ and 0.1) and three different ζ_3 ($= 0.05, 0.1$, and 0.2). There is no BS in this case. Since $B_0 \sin^2 v + B_1 \geq B_0 \sin^2 \psi_0 + B_1 = \zeta_3^2$, we can also find $L < \pi/\zeta_3$ from Eq. (24).

However, when $B_1 > 0$ Eqs. (22) and (23) can be rewritten as

$$\sqrt{B_1} s = [F(\psi|\gamma) - F(\psi_0|\gamma)], \quad (25)$$

$$\sqrt{B_1} L = F(\psi_L|\gamma) - F(\psi_0|\gamma), \quad (26)$$

$$F(\psi|\gamma) \equiv \int_0^\psi \frac{dv}{\sqrt{1 - \gamma \sin^2 v}}, \quad (27)$$

where $\gamma = -B_0/B_1$, $F(x|\gamma)$ is the elliptic integral of the first kind, and ψ_0 is determined by Eq. (26) at a specified L . It follows that $\psi = \text{am}(s'|\gamma)$ with $s' = \sqrt{B_1} s + F(\psi_0|\gamma)$ and $\text{am}(x|\gamma)$ is amplitude for Jacobi elliptic function.

IV. BISTABLE STATES

From the discussions in Sec. III B, we know that when $|B_1/B_0| \ll 1$ or $B_1/B_0 \gg 1$ or $B_1 \leq 0$, there is only one branch of solution for the static equations and the GSC of the filament is unique so that there is no BS.

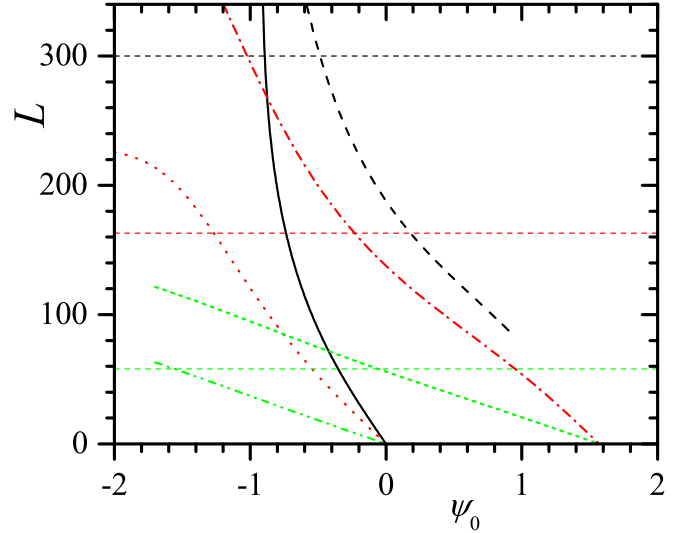


FIG. 2. L vs ψ_0 obtained from Eq. (26) when $B_0 = 0.000267$ but with different ζ_3 and n ($=0$ in left and 1 in right). The same color for the data with the same parameters. $\zeta_3 = 0.013$ (black), 0.02 (red), and 0.055 (green). Three horizontal dashed straight lines indicate the corresponding ψ_0 for BSs when $c_0 = 0.02$. The corresponding GSCs are displayed in Fig. 3. The units are the same as that in Fig. 1.

However, multiple n or multiple branches of solution is possible with a proper choice of parameters so L can be no longer a single-value function of ψ_0 . In other words, at a given L a filament can have several ψ_0 associated with different configurations but some of these configurations may have the same E . We find that the isoenergetic configurations can occur only when $n = 0$, $\psi_L = -\psi_0 > 0$ and $n = 1$, $\psi_L = \pi - \psi_0 > 0$. In other words, it can have only two isoenergetic configurations. This is because at a specified L , in general, the larger the n , the larger the $\psi_L - \psi_0$ so the larger the ψ and the higher the E .

For convenience, in this section the lines of the same color in all figures (Figs. 2–8) represent the configurations with the same parameters, i.e., in the same BS.

Our calculations show that for an individual branch, either $n = 0$ or 1 , L is still a monotonic function of ψ_0 , as shown in Fig. 2 for the filaments with $B_0 = 0.000267$ (corresponds to $b_1 = 50$, $b_3 = 75$ and $c_0 = 0.02$, i.e., the same b_1 and b_3 as that of a long dsDNA) and $\zeta_3 = 0.013, 0.02, 0.055$. When ζ_3 is small, the relations between L and ψ_0 for two branches can be quite different, shown as black or red lines in Fig. 2. But beginning from a moderate ζ_3 ($=0.055$), the relations between L and ψ_0 becomes two parallel straight lines. Note that to determine E also needs to specify c_0 and the GSC is determined by a comparison of E s among different branches. For instance, in Fig. 2, when $c_0 = 0.02$ the two different ψ_0 for GSC of a same filament are given by the crossovers between three horizontal dashed straight lines and corresponding curves with the same colors.

Moreover, the larger the c_0 or the smaller the ζ_3 , the larger the L and the larger the difference between two GSCs. Such a difference can also be characterized by the end-to-end distance $r_L = \sqrt{x^2(L) + y^2(L)}$. Four typical GSCs are displayed in Fig. 3. From Fig. 3, we can see that it is rather easy to

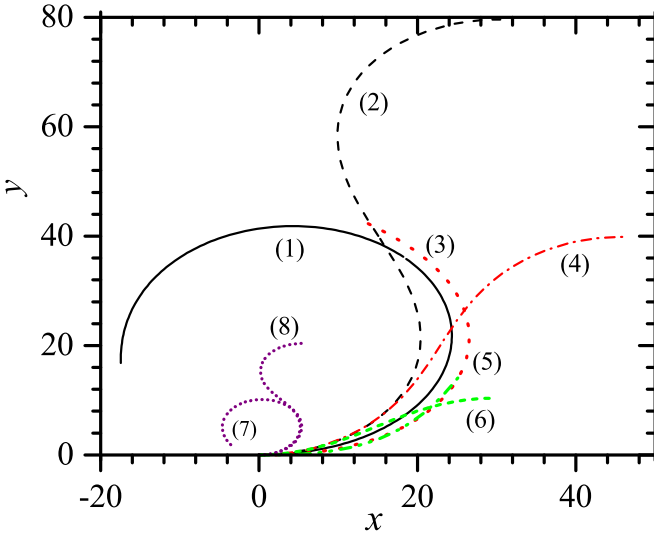


FIG. 3. GSCs in BS. The same color for the data with the same parameters. For black lines, $B_0 = 0.000267$, $c_0 = 0.02$, $\zeta_3 = 0.013$, $L = 300$, $L_h = 263.4$, and (1) $r_L = 21.7$ (solid, $n = 0$); (2) $r_L = 225.4$ (dashed, $n = 1$). For red lines, $B_0 = 0.000267$, $c_0 = 0.02$, $\zeta_3 = 0.02$, $L = 163$, $L_h = 222.1$, and (3) $r_L = 112.0$ (dotted, $n = 0$); (4) $r_L = 151.8$ (dash-dotted, $n = 1$). For green lines, $B_0 = 0.000267$, $c_0 = 0.02$, $\zeta_3 = 0.055$, $L = 58$, $L_h = 107.4$, and (5) $r_L = 56.0$ (dash-dot-dotted, $n = 0$); (6) $r_L = 57.6$ (short-dashed, $n = 1$). For purple lines, $B_0 = 0.08$, $c_0 = 0.2$, $\zeta_3 = 0.19$, $L = 28$, $L_h = 22.8$, and (7) $r_L = 3.56$ (short-dashed, $n = 0$); (8) $r_L = 21.13$ (short-dotted, $n = 1$). The units are the same as that in Fig. 1.

distinguish two isoenergetic configurations in a BS at a relative small ζ_3 , shown as black, red, and purple lines in the figure. But at a large ζ_3 , to distinguish them becomes uneasy, shown as green lines in the figure. The meaning of “large” or “small” of ζ_3 is dependent on B_0 and c_0 , and a small B_0 but a large c_0 favor a large ζ_3 . Since $\zeta_3 \approx 1.76$ for a dsDNA, $\zeta_3 = 0.19$ for the purple lines in Fig. 3 is much smaller than that of dsDNA but $c_0 = 0.2$ is already rather large. Therefore, DNA may be no a proper candidate for the BS material. Meanwhile, in BS $n = 0$ always gives an opened ringlike configuration and L is always shorter than that of a closed chain or there is not self-crossover though it can have $L > L_h$, shown as the black and purple lines in Fig. 3.

From Eq. (20), we can know that when c_0 and ζ_3 are very small, B_0 and B_1 are also small so that ψ is almost a constant and ϕ is a linear function of s , consequently the filament is in a ringlike shape and no BS. A moderate ζ_3 results in s dependent ψ , shown as black and red lines in Fig. 4. But when ζ_3 is sufficient large, ψ is close to a straight line, shown as green lines in Fig. 4. The relations between L and ζ_3 in BS are displayed in Figs. 5 and 6 and can be approximately fitted by $L = 3.3/\zeta_3$, but the smaller the ζ_3 , the larger the deviation from this approximation.

Since there is not BS at $\zeta_3 = 0$ or at a very small ζ_3 , there exists a critical ITR $\zeta_3 = \zeta_c$ and BS appears when $\zeta_3 > \zeta_c$. Figure 7 displays some typical relations between c_0 and ζ_c . From Fig. 7, we can find that the relations are almost linear and the larger the b_3 , the smaller the ζ_c . This is due to a large b_3 strengthens the role of ζ_3 . Meanwhile, the larger the c_0 ,

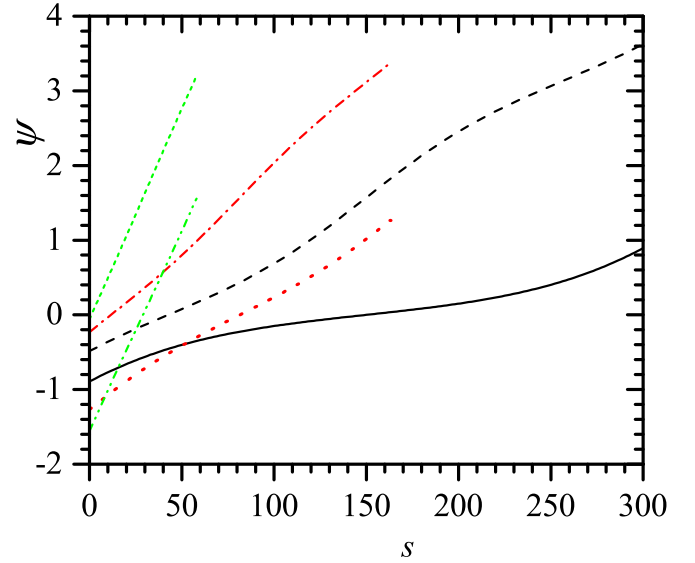


FIG. 4. ψ vs s in BS when $B_0 = 0.000267$. The same color for the data with the same parameters. $L = 300$ and $\zeta_3 = 0.013$ for solid black ($n = 0$) and dashed-black ($n = 1$) lines; $L = 163$ and $\zeta_3 = 0.02$ for red-dotted ($n = 0$) and red dash-dotted ($n = 1$) lines; $L = 58$ and $\zeta_3 = 0.055$ for green dash-dot-dotted ($n = 0$) and green short-dashed ($n = 1$) lines. The units are the same as that in Fig. 1.

the larger the ζ_c . This is also a natural result since c_0 favors a circle so at a large c_0 it requires a large ζ_3 to open the circle.

In above calculations we focus on the GSC since it can be obtained directly from the static equations together with a comparison of energies in different configurations. However, owing to the multiple solutions of static equations, even the filament has a unique GSC, it is still possible to exist some metastable solutions if these solutions have local minimum

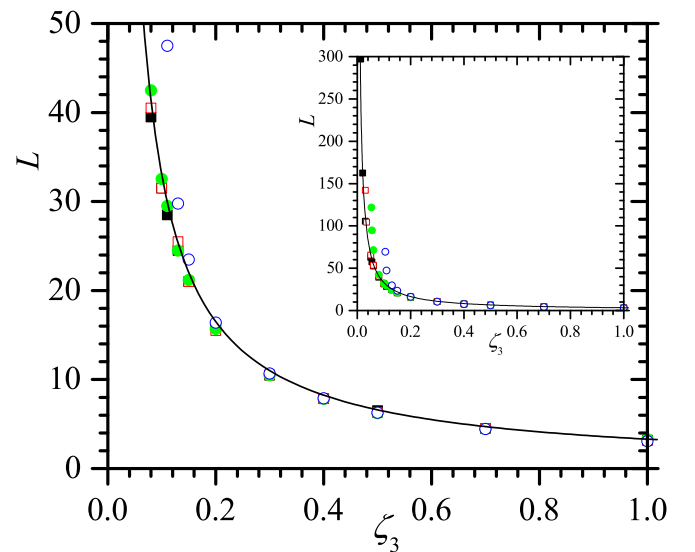


FIG. 5. L vs ζ_3 in BS when $b_3/b_1 = 1.5$. $c_0 = 0.02$ (solid black square), 0.05 (empty red square), 0.1 (solid green circle), and 0.2 (empty blue circle). The solid black lines are given by $L = 3.3/\zeta_3$. The inset presents the data with larger range in L . The units are the same as that in Fig. 1.

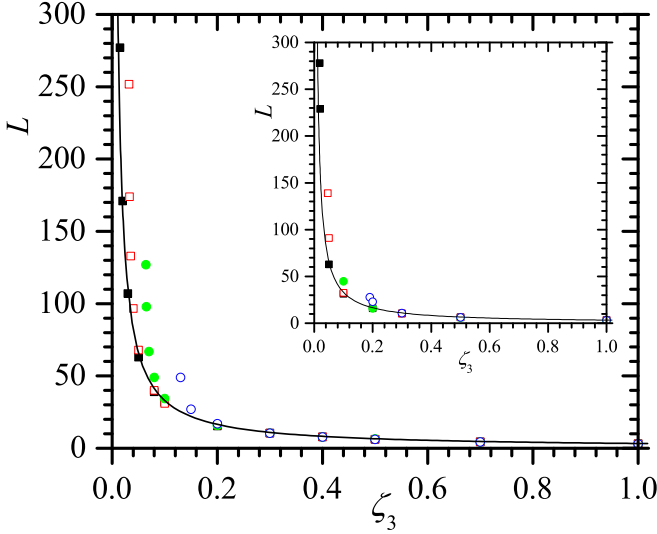


FIG. 6. L vs ζ_3 in BS when $b_3/b_1 = 1$ and $1/2$ (inset). $c_0 = 0.02$ (solid black square), 0.05 (empty red square), 0.1 (solid green circle), and 0.2 (empty blue circle). The solid black lines are given by $L = 3.3/\zeta_3$. The units are the same as that in Fig. 1.

energies. At least, if the parameters (b_i , c_0 , ζ_3 , and L) of a filament are close to that of a bistable filament, then one of the solutions must give a metastable state since its E must be very close to that of the GSC. These metastable states may be as important as the GSC because they may have some special properties and thermal fluctuation may favor these states. But how to identify the metastable state is yet a problem because it is uneasy to justify whether the solution has the maximum or the local minimum E .

We should stress that it does not need any external force or costs no energy to obtain and maintain the BS, i.e., we find a natural BS. Moreover, though to compare with the results at a finite T we adopt nm as the unit of length in this section, in

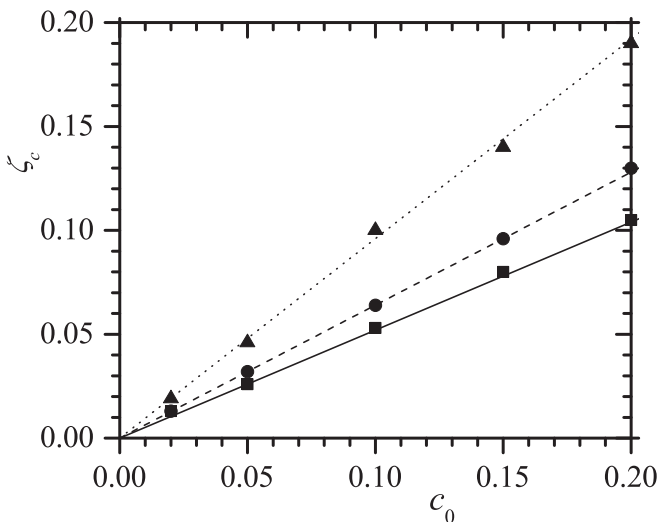


FIG. 7. ζ_c vs c_0 when $b_3/b_1 = 1.5$ (square), 1 (circle), and $1/2$ (triangle). The solid straight line is given by $\zeta_c = 0.52c_0$; the dashed straight line is given by $\zeta_c = 0.64c_0$; the dotted straight line is given by $\zeta_c = 0.96c_0$. The units are the same as that in Fig. 1.

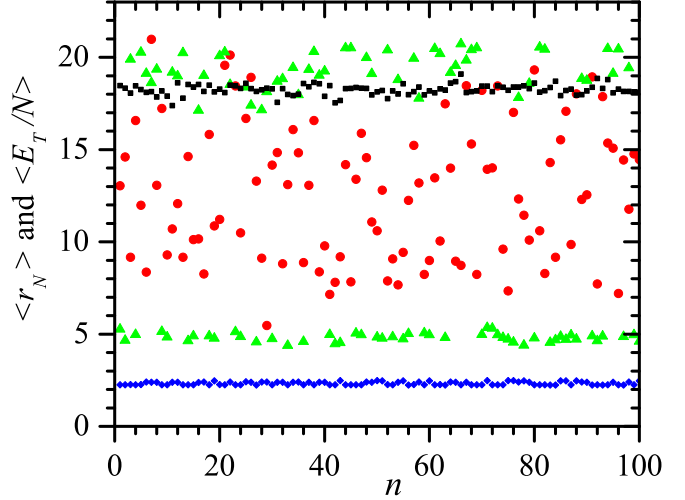


FIG. 8. $\langle r_N \rangle$ and $\langle E_T \rangle/N$ vs sample counts when $c_0 = 0.2$, $\zeta_3 = 0.19$ and $N = 28$. Black square for $\langle r_N \rangle$ when $k_1 = 12$ and $k_3 = 6$; red circle for $\langle r_N \rangle$ when $k_1 = 100$ and $k_3 = 50$; green triangle for $\langle r_N \rangle$ when $k_1 = 200$ and $k_3 = 100$. Blue diamond for $\langle E_T \rangle/N$ when $k_1 = 200$ and $k_3 = 100$. The units are the same as those described in the caption of Fig. 1.

fact such a unit is unnecessary owing to that BS is dependent on the ratio b_1/b_3 . In other words, all conclusions in this section are still correct if we replace nm by arbitrary unit of length and it is also unnecessary to care about the values of b_1 and b_3 separately.

V. EFFECTS OF THERMAL FLUCTUATION

The results in Sec. III ignore the thermal fluctuation so the stability of the BS may be problematic for a microscopic filament with a small energy barrier between two isoenergetic configurations. Moreover, the filament with a BS is always short so it may be out of the continuous model. It is also significant to justify whether the metastable state exists or not. Therefore, to clarify these questions we perform MC simulation on the discrete model.

Since this section focuses on a microscopic object, the unit of length is taken as nm so that the units of k_1 and k_3 are nm, the units of c_0 and ζ_3 are nm^{-1} , and the units of b_1 and b_3 are $k_B T_r \cdot \text{nm}$. Our results show that both isoenergetic configurations in a BS can be observed at a finite T , and large k_i s help to keep the filament to stay in one of two configurations. However, the thermal fluctuation can mix two isoenergetic configurations when k_i s are small or $L(=N)$ is large. Moreover, BLS can exist and it may be uneasy to distinguish BLS and BS at a finite T .

Figure 8 presents $\langle r_N \rangle$ and $\langle E_T \rangle$ of 100 samples with 3 sets of k_1 ($= 12, 100, 200$) and k_3 ($= 6, 50, 100$) as well as the same c_0 , ζ_3 and L as that of the purple lines in Fig. 3, i.e., $c_0 = 0.2$, $\zeta_3 = 0.19$ and $L = N = 28$. In this case, indeed $\langle E_T \rangle$ is almost the same for all samples. For instance, $\langle E_T \rangle/N \approx 2.25$ for all samples when $k_1 = 200$, $k_3 = 100$, as we can see from the blue diamonds in Fig. 8. In contrast, the behavior of $\langle r_N \rangle$ is dependent clearly on the magnitude of k_i . When k_i s are rather large, $\langle r_N \rangle$ oscillates slightly around two distinct values,

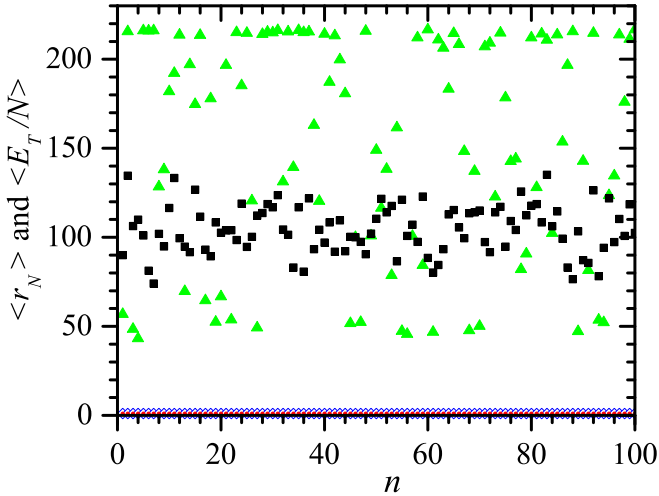


FIG. 9. $\langle r_N \rangle$ and $\langle E_T \rangle/N$ vs sample counts when $c_0 = 0.02$, $\zeta_3 = 0.013$ and $N = 300$. Green triangle for $\langle r_N \rangle$ when $k_1 = 1000$ and $k_3 = 1500$; black square for $\langle r_N \rangle$ when $k_1 = 10$ and $k_3 = 15$; blue open diamond for $\langle E_T \rangle/N$ when $k_1 = 1000$ and $k_3 = 1500$; red circle for $\langle E_T \rangle/N$ when $k_1 = 10$ and $k_3 = 15$. The units are the same as those described in the caption of Fig. 1.

such as $\langle r_N \rangle \approx 4.8$ and 19.0 when $k_1 = 200$ and $k_3 = 100$, shown as the green triangles in Fig. 8. The larger the k_i , the smaller the uncertainty of $\langle r_N \rangle$. It conforms that the filament can have two isoenergetic but distinct configurations and the filament can stay stable at one of two configurations at a finite T , as well as the thermal fluctuation has small effect in this case. In comparison, recalling that the purple lines in Fig. 3 have $r_L = 3.56, 21.13$ and $E/L \approx 1.33$, we know that due to the thermal fluctuation, the configuration with a small r_N expands but the configuration with a large r_N contracts, and $\langle E \rangle$ increases. However, the uncertainty in $\langle r_N \rangle$ increases with decreasing k_i . For instance, when $k_1 = 100$ and $k_3 = 50$, $\langle r_N \rangle$ scatters in a range $20.99 \geq \langle r_N \rangle \geq 5.47$, shown as the red circles in Fig. 8. In this case, the fact that $\langle E_T \rangle/N$ is still almost the same for all samples suggests that the energy barrier between two configurations is comparable to $k_b T$ so that the filament can shift between two configurations and results in a large uncertainty in $\langle r_N \rangle$. Moreover, when k_i s are quite small, the energy barrier becomes smaller than $k_b T$ so the filament is like a WLC and $\langle r_N \rangle$ converges to a unique value, shown as the black squares in Fig. 8 when $k_1 = 12$ and $k_3 = 6$. In this case, $\langle r_N \rangle \approx 18$ so is closer to the larger $r_L (= 21.13)$.

The finite size effect is quite serious at a finite T and Fig. 9 displays some typical results of $\langle r_N \rangle$ and $\langle E_T \rangle$ from 100 samples with 2 sets of k_1 ($= 10, 1000$) and k_3 ($= 15, 1500$) as well as the same c_0, ζ_3 and L as that of the black lines in Fig. 3, i.e., $c_0 = 0.02$, $\zeta_3 = 0.013$, $L = 300$, $r_L = 21.7$, and 225.4 . Again, $\langle E_T \rangle$ is almost the same for all samples, shown as blue open diamonds and red circles in Fig. 9. Similar to that in Fig. 8, at small k_i s $\langle r_N \rangle$ tends to converge to a unique value, shown as the black squares in Fig. 9 when $k_1 = 10$ and $k_3 = 15$, and average over 100 samples we obtain $\langle r_N \rangle \approx 104$ so is very closer to the mean of two r_L s. It reveals that two isoenergetic configurations have the same opportunity to

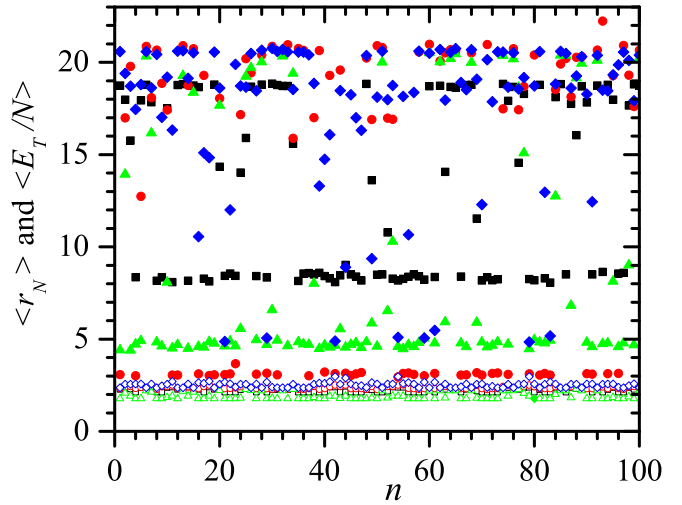


FIG. 10. $\langle r_N \rangle$ (solid) and $\langle E_T \rangle/N$ (empty) vs sample counts in BLS when $k_1 = 200$, $k_3 = 100$, and $c_0 = 0.2$. Black square for $N = 23$ and $\zeta_3 = 0.19$; red circle for $N = 33$ and $\zeta_3 = 0.19$; green triangle for $N = 28$ and $\zeta_3 = 0.15$; blue diamond for $N = 28$ and $\zeta_3 = 0.22$. The units are the same as those described in the caption of Fig. 1.

appear. Whether the shift between two configurations has a regular frequency is an intrigue topic since such a system can become a potential high frequency oscillator so that the dynamics of the system deserves a further study. The thermal effect is much more serious than that for a short chain since $\langle r_N \rangle$ is clearly sample dependent in this case. Larger k_i s tend to separate two isoenergetic configurations but serious thermal effect prevents the tendency so we can see that $\langle r_N \rangle$ scatters in a range $216.6 \geq \langle r_N \rangle \geq 43.2$ or it shifts between two configurations up to $k_1 = 1200$ and $k_3 = 1800$, shown as green triangles in Fig. 9. Moreover, if the difference between two configurations is small, then at a finite T two configurations become indistinguishable even the filament is not too long, such as that presented as the green lines in Fig. 3 when $c_0 = 0.02$, $\zeta_3 = 0.055$, and $L = 58$.

We find further that there are indeed some metastable states. Figure 10 demonstrates $\langle r_N \rangle$ and $\langle E_T \rangle$ of 100 samples with the same k_1, k_3 , and c_0 as that of the green triangles in Fig. 8 but slightly different N ($= 23, 28$, and 33) or ζ_3 ($= 0.15, 0.19$, and 0.22). From Fig. 10 we can observe clearly two distinct configurations, such as the red circles and the green triangles in figure. Figure 10 also shows the shift of $\langle r_N \rangle$ between two configurations though $\langle E_T \rangle$ still keeps almost the same for all samples. Comparing with the green triangles in Fig. 8, we know that these metastable states should be less stable than that obtained from the GSC since $\langle r_N \rangle$ has clearly a larger uncertainty. These results also suggest that BLS may be indistinguishable from BS at a finite T so that they may be equal important in practical applications. It therefore extends the range of parameters for BS so to make it be more feasible to find and make some new bistable materials.

From above results, we know that to maintain the filament in one of two distinct configurations at a finite T requires sufficient large k_i . Since $k_i \equiv b_i/d_0 k_B T$, larger k_i can be obtain by either increasing b_i or decreasing T . Moreover, the results

from the continuous model are still valid and instructive at a finite T .

VI. CONCLUSIONS AND DISCUSSIONS

In summary, we find a new bistable mechanism, i.e., the couple and competition between ITR and IR can induce a BS for a 2D filament even the filament is free of the external force because there are multiple solutions for the static equations of GSC. This new phenomenon is different completely from its 3D counterpart that has a unique helical GSC. There are two configurations of equal energy in a BS and these isoenergetic configurations, one of which is in a ringlike shape, have different shapes and end-to-end distances. The smaller the ITR or the larger the IC, the more obvious the distinction between two isoenergetic configurations and the longer the filament. In BS, the relation between L and ITR is approximately a hyperbola and the relation between IC and critical ITR is approximately linear. L of a BS is always shorter than that of a closed chain or there is no self-crossover. The Monte Carlo simulation at a finite T suggests that the energy barrier between two isoenergetic configurations in a BS may be comparable to $k_B T$ so that the filament can shift between two isoenergetic configurations but large k_1 and k_3 can prevent such a shift and keep the filament staying in one of two configurations. The simulation also reveals the existence of BLS and suggests that the BLS should be a common phenomenon for a 2D filament due to the multiple solutions is quite common for the static equations.

The requirement of a large k_1 and k_3 to maintain the filament at a specified configuration at a finite T may make it difficult to realize. To overcome this problem one can enhance the bending and twisting rigidities or lower T or apply a small force. Clearly a small force can help to fix the filament in one configuration and change the direction of force can result in a transformation between two configurations, so that applying an appropriate force may be a more practical way to control the configuration of the filament.

Though our findings are valid for both macroscopic and microscopic filaments, we have to point out that it is uneasy to realize a 2D short macroscopic filament when it has both finite ITR and IC since its natural shape in 3D space is a helix so requires a strong compressive force to press it to a plane. Therefore, our findings should be more practicable for a microscopic filament. Moreover, since 2D and 3D filaments exhibit different properties, we can expect that BS should also exist in some strongly confined systems or in some quasi-2D systems. To realize a quasi-2D system is not too difficult and should be more practical since the adsorptive force from the substrate tends to compress the filament to the surface so makes a nearly planar system, as we can see from some experiments [17–19,29]. Finally, our findings also suggest that in a crowd environment, an intrinsically curved and twisted filament may exhibit very different property from its 3D counterpart and it should be also very important for some macroscopic filaments, such as filaments in some composite materials or smart materials.

-
- [1] C. J. Benham, *Phys. Rev. A* **39**, 2582 (1989).
 - [2] J. F. Marko and E. D. Siggia, *Science* **265**, 506 (1994).
 - [3] C. Bouchiat and M. Mézard, *Phys. Rev. Lett.* **80**, 1556 (1998).
 - [4] C. Bustamante, J. F. Marko, E. D. Siggia, and S. Smith, *Science* **265**, 1599 (1994).
 - [5] J. F. Marko and E. D. Siggia, *Macromolecules* **28**, 8759 (1995).
 - [6] C. Bouchiat, M. D. Wang, J. F. Allemand, T. Strick, S. M. Block, and V. Croquette, *Biophys. J.* **76**, 409 (1999).
 - [7] B. Fain, J. Rudnick, and S. Östlund, *Phys. Rev. E* **55**, 7364 (1997).
 - [8] B. Fain and J. Rudnick, *Phys. Rev. E* **60**, 7239 (1999).
 - [9] S. V. Panyukov and Y. Rabin, *Phys. Rev. E* **64**, 011909 (2001).
 - [10] S. K. Nomidis, M. Caraglio, M. Laleman, K. Phillips, E. Skoruppa, and E. Carlon, *Phys. Rev. E* **100**, 022402 (2019).
 - [11] T. Curk, J. D. Farrell, J. Dobnikar, and R. Podgornik, *Phys. Rev. Lett.* **123**, 047801 (2019).
 - [12] S. Das and A. Cacciuto, *Phys. Rev. Lett.* **123**, 087802 (2019).
 - [13] S. K. Nomidis, E. Skoruppa, E. Carlon, and J. F. Marko, *Phys. Rev. E* **99**, 032414 (2019).
 - [14] H. Yamakawa and T. Yoshizaki, *Helical Wormlike Chains in Polymer Solutions* (Springer-Verlag, Berlin, 1996).
 - [15] A. Goriely and M. Tabor, *Proc. R. Soc. London A* **453**, 2583 (1997).
 - [16] H. R. Drew and A. A. Travers, *J. Mol. Biol.* **186**, 773 (1985).
 - [17] M. Dlakic, K. Park, J. D. Griffith, S. C. Harvey, and R. E. Harrington, *J. Biol. Chem.* **271**, 17911 (1996).
 - [18] W. Han, S. M. Lindsay, M. Dlakic, and R. E. Harrington, *Nature (London)* **386**, 563 (1997).
 - [19] W. Han, M. Dlakic, Y. J. Zhu, S. M. Lindsay, and R. E. Harrington, *Proc. Natl. Acad. Sci. U.S.A.* **94**, 10565 (1997).
 - [20] R. E. Goldstein, A. Goriely, G. Huber, and C. W. Wolgemuth, *Phys. Rev. Lett.* **84**, 1631 (2000).
 - [21] S. V. Panyukov and Y. Rabin, *Phys. Rev. E* **62**, 7135 (2000).
 - [22] B. Smith, Y. V. Zastavker, and G. B. Benedek, *Phys. Rev. Lett.* **87**, 278101 (2001).
 - [23] D. A. Kessler and Y. Rabin, *Phys. Rev. Lett.* **90**, 024301 (2003).
 - [24] Z. Zhou, P.-Y. Lai, and B. Joós, *Phys. Rev. E* **71**, 052801 (2005).
 - [25] A. Scipioni, C. Anselmi, G. Zuccheri, B. Samori, and P. De Santis, *Biophys. J.* **83**, 2408 (2002).
 - [26] G. Zuccheri, A. Scipioni, V. Cavaliere, G. Gargiulo, P. De Santis, and B. Samor, *Proc. Natl. Acad. Sci. U.S.A.* **98**, 3074 (2001).
 - [27] S. Rappaport and Y. Rabin, *Macromolecules* **37**, 7847 (2004).
 - [28] C. Vaillant, B. Audit, and A. Arnéodo, *Phys. Rev. Lett.* **95**, 068101 (2005).
 - [29] J. Moukhtar, E. Fontaine, C. Faivre-Moskalenko, and A. Arnéodo, *Phys. Rev. Lett.* **98**, 178101 (2007).
 - [30] E. L. Starostin and G. H. M. van der Heijden, *Phys. Rev. Lett.* **101**, 084301 (2008).
 - [31] S. K. Nomidis, F. Kriegel, W. Vanderlinden, J. Lipfert, and E. Carlon, *Phys. Rev. Lett.* **118**, 217801 (2017).
 - [32] D. Grossman, E. Sharon, and E. Katzav, *Phys. Rev. E* **98**, 022502 (2018).

- [33] M. Pezulla, N. Stoop, M. P. Steranka, A. J. Bade, and D. P. Holmes, *Phys. Rev. Lett.* **120**, 048002 (2018).
- [34] G. T. Vu, A. A. Abate, L. R. Gómez, A. D. Pezzutti, R. A. Register, D. A. Vega, and F. Schmid, *Phys. Rev. Lett.* **121**, 087801 (2018).
- [35] S. Iijima, *Nature (London)* **354**, 56 (1991); S. Iijima, T. Ichihashi, and Y. Ando, *ibid.* **356**, 776 (1992).
- [36] X. B. Zhang, *Europhys. Lett.* **27**, 141 (1994).
- [37] M.-F. Yu, M. J. Dyer, J. Chen, D. Qian, W. K. Liu, and R. S. Ruoff, *Phys. Rev. B* **64**, 241403(R) (2001).
- [38] A. F. da Fonseca and D. S. Galvão, *Phys. Rev. Lett.* **92**, 175502 (2004).
- [39] V. R. Coluci, A. F. Fonseca, D. S. Galvão, and C. Daraio, *Phys. Rev. Lett.* **100**, 086807 (2008).
- [40] J.-S. Wang, Y.-H. Cui, X.-Q. Feng, G.-F. Wang, Q.-H. Qin, *Europhys. Lett.* **92**, 16002 (2010).
- [41] Z. Zhou, *Phys. Rev. E* **102**, 032405 (2020).
- [42] Z. Zhou, F.-T. Lin, C.-Y. Hung, H.-Y. Wu, and B.-H. Chen, *J. Phys. Soc. Jpn.* **83**, 044802 (2014).
- [43] Z. Zhou, *J. Phys. Commun.* **2**, 035008 (2018).
- [44] S. C. Bae, F. Xie, S. Jeon, and S. Granick, *Curr. Opin. Solid State Mater. Sci.* **5**, 327 (2001).
- [45] N. Iwai, K. Nagai, and M. Wachi, *Biosci. Biotechnol. Biochem.* **66**, 2658 (2002).
- [46] B. Maier, U. Seifert, and J. O. Radler, *Europhys. Lett.* **60**, 622 (2002).
- [47] Z. Gitai, N. Dye, and L. Shapiro, *Proc. Natl. Acad. Sci. U.S.A.* **101**, 8643 (2004).
- [48] A. Prasad, Y. Hori, and J. Kondev, *Phys. Rev. E* **72**, 041918 (2005).
- [49] Z. Zhou, *Phys. Rev. E* **76**, 061913 (2007).
- [50] Z. Zhou and B. Joós, *Phys. Rev. E* **80**, 061911 (2009).
- [51] I. Živić, S. Elezović-Hadžić, and S. Milošević, *Phys. Rev. E* **98**, 062133 (2018).
- [52] Jeff Z. Y. Chen, *Phys. Rev. Lett.* **121**, 037801 (2018).
- [53] D. A. Matoz-Fernandez, D. H. Linares, and A. J. Ramirez-Pastor, *Europhys. Lett.* **82**, 50007 (2008).
- [54] P. Longone, D. H. Linares, and A. J. Ramirez-Pastor, *J. Chem. Phys.* **132**, 184701 (2010).
- [55] Y.-C. Wang, and E. L. Ferguson, *Nature* **434**, 229 (2005).
- [56] H. Shin, S. Seo, C. Park, J. Na, M. Han, and E. Kim, *Energy Environ. Sci.* **9**, 117 (2016).
- [57] W. Zhang, X. Wang, Y. Wang, G. Yang, C. Gu, W. Zheng, Y.-M. Zhang, M. Li, and S. X.-A. Zhang, *Nat. Commun.* **10**, 1559 (2019).
- [58] Y. Wang, S. Wang, X. Wang, W. Zhang, W. Zheng, Y.-M. Zhang, and S. X.-A. Zhang, *Nat. Mater.* **18**, 1335 (2019).
- [59] H. Goldstein, *Classical Mechanics*, 3rd ed. (Addison-Wesley, Boston, MA, 2002).
- [60] B. Audit, C. Thermes, C. Vaillant, Y. d'Aubenton-Carafa, J. F. Muzy, and A. Arnéodo, *Phys. Rev. Lett.* **86**, 2471 (2001).
- [61] C. Vaillant, B. Audit, C. Thermes, and A. Arnéodo, *Eur. Phys. J. E* **19**, 263 (2006).
- [62] Y. Lu, B. Weers, and N. C. Stellwagen, *Biopolymers* **61**, 261 (2002).
- [63] D. P. Landau and K. Binder, *A Guide to Monte Carlo Simulations in Statistical Physics*, 2nd ed. (Cambridge University Press, Cambridge, UK, 2005).